JME

Journal of Mining & Environment,
Vol.6, No.2, 2015, 225-236.

Prediction of mineral deposit model and identification of mineralization trend in depth using frequency domain of surface geochemical data in Dalli Cu-Au porphyry deposit

H. Shahi[1]*, S.R. Ghavami Riabi[1], A. Kamkar Rouhani[1] and H. Asadi Haroni[2]

1. School of Mining, Petroleum & Geophysics Engineering, Shahrood University of Technology, Shahrood, Iran
2. Mining Faculty, Isfahan University of Technology, Isfahan, Iran

Received 12 November 2014; received in revised form 3 January 2015; accepted 6 April 2015
**Corresponding author: hssn.shahi@gmail.com (H. Shahi).*

Abstract
In this research work, the frequency domain (FD) of surface geochemical data was analyzed to decompose the complex geochemical patterns related to different depths of the mineral deposit. In order to predict the variation in mineralization in the depth and identify the deep geochemical anomalies and blind mineralization using the surface geochemical data for the Dalli Cu-Au porphyry deposit, a newly developed approach was proposed based on the coupling Fourier transform and principal component analysis. The surface geochemical data was transferred to FD using Fourier transformation and high and low pass filters were performed on FD. Then the principal component analysis method was employed on these frequency bands separately. This new combined approach demonstrated desirably the relationship between the high and low frequencies in the surface geochemical distribution map and the deposit depth. This new combined approach is a valuable data-processing tool and pattern-recognition technique to identify the promising anomalies, and to determine the mineralization trends in the depth without drilling. The information obtained from the exploration drillings such as boreholes confirms the results obtained from this method. The new exploratory information obtained from FD of the surface geochemical distribution map was not achieved in the spatial domain. This approach is quite inexpensive compared to the traditional exploration methods.

Keywords: *Principal Component Analysis, Frequency Domain (FD), 2D Fourier Transformation, Blind Mineralization, Pattern Recognition.*

1. Introduction

The geo-chemical interpretations are usually carried out in the spatial domain. In addition to the spatial domain methods for anomaly separation, the frequency domain (FD) of the geochemical data has been used to decompose the complex geo-chemical patterns and separate the syngenetic component related to very low frequencies from anomalous factors. The power spectrum-area (SA) fractal method has been applied for the separation of geochemical patterns on the basis of distinct self-similarity in FD of the geochemical data [1-10]. The SA fractal method can decompose the complex geochemical patterns into anomalies and backgrounds. The Fourier method is the most powerful technique used for signal analysis. It transforms the signal from the time domain or spatial domain to FD, in which many characteristics of the signal are revealed [6].

Grigorian has propounded a zonality model in the spatial domain to recognize a blind mineralization zone from a dispersed mineralization one [11, 12]. Several methods have been performed to determine the hidden ore bodies in the spatial domain of geochemical data based on the horizons of the erosional surface [11-16]. Ziaii et al. have successfully separated a dispersed mineralization from blind mineralization using the neuro-fuzzy modeling-based genetic algorithms [17].

To investigate the mineralization characteristics and to identify the mineralization factor(s), the

PCA method has frequently been applied to the analysis of geochemical and geo science data [18-21].

PCA is a multivariate statistical method for the geo-information identification and integration of geo-datasets [22]. Correlated variables in geo-datasets with high dimensionality are transformed into several uncorrelated principal components (PCs) based on a covariance or correlation matrix [23]. The reduced number of PCs obtained increases the interpretability of the information available for specific objectives [24]. In this research work, in order to determine the exploratory features of the geochemical data from the Dalli area in different frequencies, the high-pass and low-pass filters are performed on FD of geochemical data based on the wave number values, and the principal component analysis (PCA) method is employed on these different frequency bands separately, and as a result, the mineralization components are evaluated.

2. Geological particulars, alteration,and mineralogical structure in studied area

The Dalli porphyry deposit was formed in the Uremia–Dokhtar magmatic belt, which is located in the central Iran [25, 26]. In this belt, the plutonic rocks mostly include diorite, granodiorite, and granitoid, and the oligo-Miocene volcanic rocks include andesite, dacite, and pyroclastics. The mineralized Cu-Au zone in this area was formed in the igneous diorite, quartz diorite porphyry (QDP), and the volcanic rocks such as porphyritic amphibole andesite, andesite, dacite, and pyroclastics were formed during the late Miocene to Pliocene (Figure 1) [27]. There are different types of alterations such as potassic, propylitic, silicic, and locally phyllic in the Dalli area. The potassic alteration was formed during the tonalitic intrusion that includes a high amount of mineralization, consisting of quartz-potassium, feldspar-magnetite, and biotite. Potassic alteration occurred in the center of the area, and was progressively surrounded by the sericitic, sericite-chlorite, and propylitic alteration zones towards the border in the porphyry deposits. In the QDP and andesite rocks, the Cu-Au mineralization is related to the potassic-phyllic and propylitic-silicic alteration zones, respectively. Mineralization in the northern part of Dalli occurs in the granodiorite plutonic complex (tonalite), quartz diorite, and andesite rocks. The QDP rocks indicate a high quartz-magnetite vein and a mineralization with high potassic alteration. Mineralization in the northern Dalli occurs in the quartz veins as a stockwork. Chalcopyrite is the main sulfide mineral, and pyrite and bornite also exist in the studied area. Malachite, iron oxide, pyrite, and chalcopyrite can also be observed in the drilled trenches. The supergene, transition, and hypogene zones have been identified using malachite, native Cu, and bornite. Molybdenum increases near the center of the granodiorite intrusion. The potassic alteration includes gold, bornite, chalcopyrite, pyrite, magnetite, hematite±sericite, biotite, and quartz [25].

3. Fourier transform

Two-dimensional Fourier transform (2D-FT) allows us to represent and interpret the spatial data such as the images in FD [28]. The spatial domain responses can be considered as superimposed signals of different frequencies [7]. The spatial data can be transferred to FD, based on 2D-FT [29, 30], which decomposes the signals to different frequencies. Fourier transformation decomposes the signals into different frequencies. One of the equations used to conduct FT has been presented by Dobrin and Savit [31]:

$$F(K_x, K_y) = \int_{-\infty}^{\infty}\int_{-\infty}^{\infty} f(x,y)\cos(K_x x + K_y y)dxdy - i\int_{-\infty}^{\infty}\int_{-\infty}^{\infty} f(x,y)\sin(K_x x + K_y y)dxdy \quad (1)$$

Where f(x,y) is the signal in the spatial domain, K_x and K_y are "wave numbers" with respect to the x and y axes. Wave number is the spatial counterpart of frequency, increasing proportional to wavelengths, as follows:

$$\lambda_x = 2\pi / K_x \quad \text{and} \quad \lambda_y = 2\pi / K_y, \quad \text{or} \quad \lambda = 2\pi\sqrt{(1/K_x^2 + 1/K_y^2)} \quad (2)$$

Therefore, the function f(x,y) in the spatial domain, which is the geochemical map in this study, can be converted to $F(K_x,K_y)$. It consists of the real and imaginary parts $R(K_x,K_y)$ and $I(K_x, K_y)$, respectively. The power spectrum is defined based on the following equation [32, 33]:

$$E(K_x, K_y) = R^2(K_x, K_y) + I^2(K_x, K_y) \quad (3)$$

In FD, we have the power spectrum values and wave numbers in the X and Y directions instead of the geochemical map of the elements.

Processing of the geo science data in FD often involves operations such as filtering and reducing the noise from signal [34]. The filter function, $G(K_x,K_y)$, can modify the functions $R(K_x,K_y)$ and

$I(K_x,K_y)$ by multiplying, so that some ranges of wave numbers can be eliminated and others enhanced [18]. Therefore, the filter function represents the decomposed function. Signal patterns are enhanced in certain frequencies and eliminated in the others. It can be applied to the geochemical anomaly separation. The conventional filters in physics, electrical engineering, and geophysics include the low-pass, high-pass, band pass, and directional band pass filters [18]. A low-pass filter generally eliminates the signals with high frequencies, and a high-pass filter eliminates low frequencies. These filters may be performed on the K_x-K_y map only based on the wave number values, without considering the power-spectrum values [35].

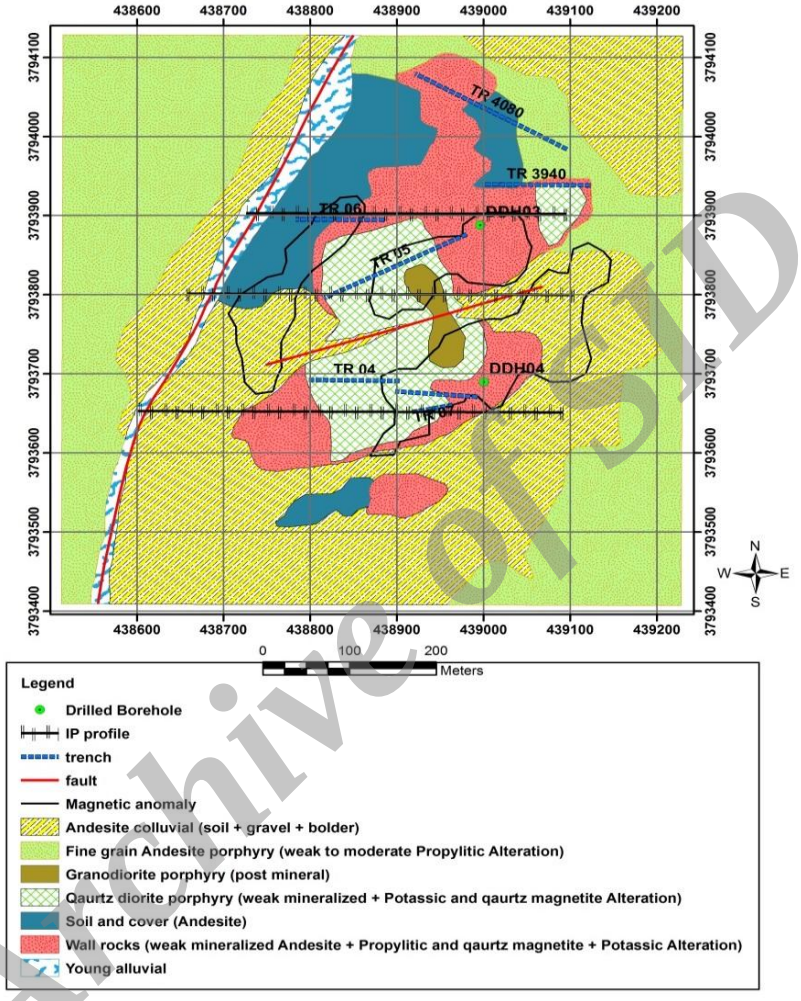

Figure 1. Geological map of northern part of Dalli area (scale 1:1000) [27].

4. Discussion

Through systematic soil sampling, a grid net of 50×50 $m^2$was used for sampling (Figure 2). 165 samples with a size fraction of −200 mesh were collected and analyzed for 30 elements using the ICP-MS method.

In this research work, a new combined approach was represented to predict and delineate the mineralization trend in the depth using FD of the surface geochemical data. The implementation of this scenario was defined, step by step, as follows:

Step 1: Transformation of the geochemical data for all the elements, separately, from the spatial domain to FD using 2D-FT.

Step 2: Designing filter functions based on the wave numbers obtained in the X and Y directions and power spectrum values.

Step 3: Applying the filter functions on the FD data, and separating the frequency bands from each other.

Step 4: Analysis of the frequency bands using the PCA method, identification of the mineralization factor, and surveying the relationship between the mineralization elements in different frequency bands.

Step 5: Delineation of the mineralization trend, and variation in the concentrations from surface to

depth using the mineralization factors of frequency bands obtained based on the high-, low-, and band-pass filters.

The spatial domain geochemical data for 30 elements was transferred to FD using 2D-FT. The FD data included the wave numbers in the x and y directions and their power spectrum (PS) values. The power spectrum (PS) map created from the molybdenum content values is shown in Figure3 to illustrate the application of the high-, low-, and band-pass filters, and distribution of the PS values. High values of PS were mainly distributed around the center of the map, corresponding to low frequencies. In general, the PS values decreased, moving away from the center.

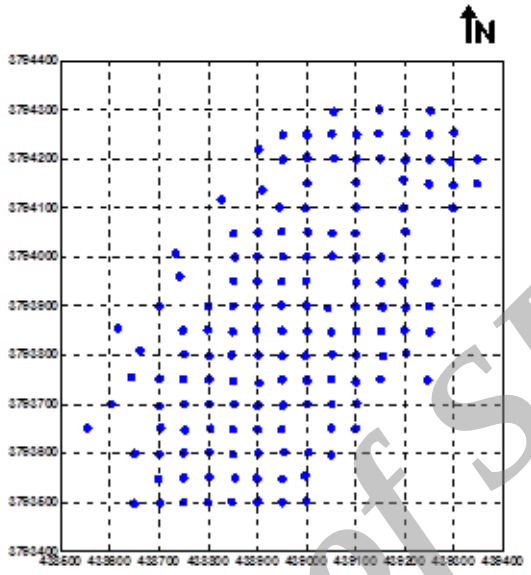

Figure 2. Blank sheet of soil sample locations in northern part of Dalli area.

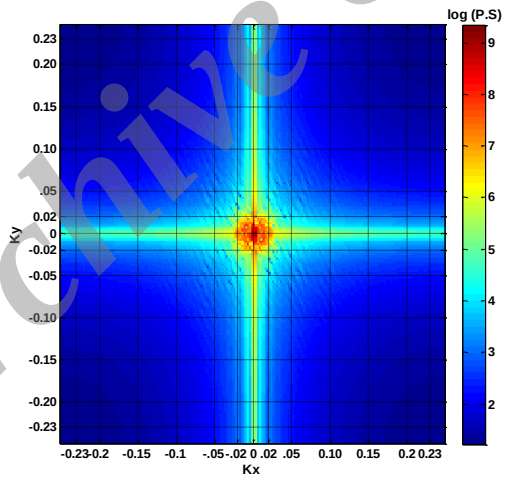

Figure 3. Molybdenum PS map obtained by Fourier transformation.

The geochemical halos of the mineral deposits at different depths cause various frequencies in the surface geochemical distribution map. In order to survey the mineralization features, and determine the elements related to the mineralizing phase in the deferent frequency bands, a newly-developed approach was proposed based on coupling 2D-FT and PCA. Therefore, 10 frequency bands were considered based on the wave number values (Table 1). These high-, band-, and low-pass filters were performed on FD of the geochemical data for 30 elements. The filters 3 and 5 on the molybdenum PS map were depicted in Figure 4. Therefore, these filters were used based on the wave number values in the X and Y directions. The high-pass filters preserve the high frequencies related to the high wave number values, and the low-pass filters preserve the low frequencies. The filter function $G(K_x,K_y)$ modify the function $E(K_x,K_y)$ by multiplying, so that some ranges of wave numbers are eliminated and the others enhanced.

Table1. Frequency bands and their applied filters on FD of geochemical data.

Frequency	Filter
Band 1	$G(k_x,k_y)=\begin{cases}1 & \lvert k_x\rvert \geq 0.23 \quad \text{and} \quad \lvert k_y\rvert \geq 0.23 \\ o & \text{otherwise}\end{cases}$
Band 2	$G(k_x,k_y)=\begin{cases}1 & \lvert k_x\rvert \geq 0.20 \quad , \quad \lvert k_y\rvert \geq 0.20 \\ o & \text{otherwise}\end{cases}$
Band 3	$G(k_x,k_y)=\begin{cases}1 & \lvert k_x\rvert \geq 0.20 \quad \text{OR} \quad \lvert k_y\rvert \geq 0.20 \\ o & \text{otherwise}\end{cases}$
Band 4	$G(k_x,k_y)=\begin{cases}1 & \lvert k_x\rvert \ , \ \lvert k_y\rvert \leq 0.20 \quad \text{and} \quad \begin{cases}0.15 \leq \lvert k_x\rvert \leq 0.20 \\ \text{OR} \\ 0.15 \leq \lvert k_y\rvert \leq 0.20\end{cases} \\ 0 & \text{otherwise}\end{cases}$
Band 5	$G(k_x,k_y)=\begin{cases}1 & \lvert k_x\rvert \ , \ \lvert k_y\rvert \leq 0.15 \quad \text{and} \quad \begin{cases}0.10 \leq \lvert k_x\rvert \leq 0.15 \\ \text{OR} \\ 0.10 \leq \lvert k_y\rvert \leq 0.15\end{cases} \\ 0 & \text{otherwise}\end{cases}$
Band 6	$G(k_x,k_y)=\begin{cases}1 & \lvert k_x\rvert \ , \ \lvert k_y\rvert \leq 0.10 \quad \text{and} \quad \begin{cases}0.05 \leq \lvert k_x\rvert \leq 0.10 \\ \text{OR} \\ 0.05 \leq \lvert k_y\rvert \leq 0.10\end{cases} \\ 0 & \text{otherwise}\end{cases}$
Band 7	$G(k_x,k_y)=\begin{cases}1 & \lvert k_x\rvert \ , \ \lvert k_y\rvert \leq 0.05 \\ o & \text{otherwise}\end{cases}$
Band 8	$G(k_x,k_y)=\begin{cases}1 & \lvert k_x\rvert \ , \ \lvert k_y\rvert \leq 0.02 \\ o & \text{otherwise}\end{cases}$
Band 9	$G(k_x,k_y)=\begin{cases}1 & \lvert k_x\rvert \ , \ \lvert k_y\rvert \leq 0.005 \\ o & \text{otherwise}\end{cases}$
Band 10	$G(k_x,k_y)=\begin{cases}1 & \lvert k_x\rvert \ , \ \lvert k_y\rvert \leq 0.0025 \\ o & \text{otherwise}\end{cases}$

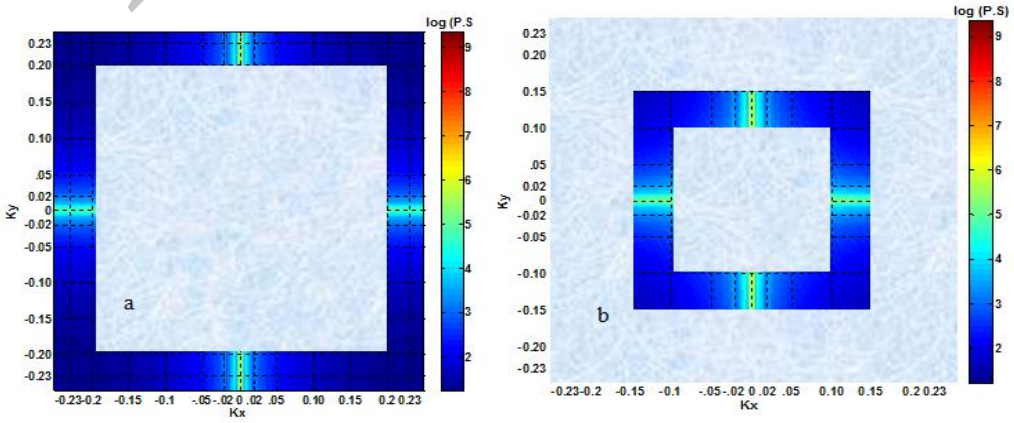

Figure 4. Molybdenum PS map obtained by Fourier transformation and applied filters in a: frequency band3; b: frequency band 5.

The PCA method was applied to the different frequency bands, separately, and the mineralization components were evaluated. The PCA method was considered based on the wave numbers and their PS values for 30 elements. The obtained results are shown in Tables 2, 3, and 4. The mineralization principal component (MPC) was specified, and the mineralization elements were highlighted for the frequency bands. A value bigger than 0.5 is an evaluation criterion for determination of the mineralization elements based on the rotated component matrix in the PCA method.

In some complicated geological environments, extraction of exploratory features in the spatial domain is impossible but these patterns become clear in FD. The frequency attributes caused by different geological processes can be useful for the identification of mineralization features. The high frequencies in the surface geochemical distribution maps may be related to the surface anomalies and geochemical noises. According to the PCA method, the high frequencies were classified into 6 and 5 principal components (PCs) in the frequency bands (FBs) 1 and 2, respectively. PC4 in FB1, which was recognized as MPC, consists of the elements Cu, Au, Cr, Ba, and Ni. MPC in FB2 concludes the elements Cu and Au. Mo is not related to Au and Cu in these high-frequency bands.

Blind and deep geochemical anomalies may create very weak and invisible effects in the surface concentration of the elements, and these assays may be less than the background values. The background patterns related to regional geological processes, and the deep and blind mineralizations can create low frequencies in the surface geochemical data. Therefore, PCA can be applied on low FBs to classify the low frequencies of the elements into the background and deep anomalies. The results of this analysis for the low FBs 6, 7, 8, and 9 desirably identified the mineralizing elements Au, Cu, and Mo, and also showed the mineralization component much better than the PCA results for the high FBs.

According to the PCA method, the 30 elements were classified into the second components in FB10 (very low frequencies). 29 elements were classified together into the first component, and Mo was in the second component, separately. Very low frequencies in the PS map did not have the effects of surface geochemical noises, while they can relate to the background values and very deep geochemical anomalies. The second principal component, which was recognized as MPC, showed a deep Mo geochemical anomaly. There is a direct relationship between the deposit depth and the frequencies of the surface geochemical distribution map. With increase in the mineralization depth, the geochemical frequencies in the surface were reduced, while the near-surface deposits usually created the high frequencies.

The MPC coefficients in the rotated component matrix in the PCA method show the importance and intensity of the elements in a mineral deposit. These MPC values, related to Au, Cu, and Mo for a variety of FBs, were extracted, and their diagrams were plotted. The MPC values *vs.* FBs in these diagrams can demonstrate the variability of anomalies in the deferent depths. Distribution of the Mo, Au, and Cu elements in the borehole DDH03, and variability of the MPC values are illustrated in Figure 5. The results obtained from the exploration drillings desirably confirm the results obtained from this new interesting idea; there is a complete compliance between them. The Au and Cu elements have a decreasing trend and Mo has an increasing trend, from FB1 to FB10 (surface to depth). This is confirmed by the results obtained for the borehole. The exploratory studies show that there is a sequence of Au (Cu)→Cu (Au)→ Mo from surface to depth in the borehole, and the mineralization zones to the wall rock.

This sequence was clearly predicted in the MPC values diagrams. The results obtained for the new approach and the boreholes clearly show the same variation in Cu, Au, and Mo in the studied area.

There was a deep Mo geochemical anomaly from 240m to down in the borehole, which is properly predicted from the MPC values diagram. The MPC values for Cu and Au show two peaks for the high and intermediate FBs related to the surface and deep anomalies. The high correlation between Cu and Au in the MPC diagram is related to their correlation in the hypogene and supergene zones. The hypogene zone was characterized by a relative increase in the Cu-Au values in the QDP rocks, and in a deeper depth, decrease in Au in the andesite rocks. The MPC values for Au strongly decreased in very low FBs (FB9 and 10),showing decrease in the Au value in the depth. This interesting result was also confirmed by the results obtained for the borehole DDH03 (Figure 5). The valuable proposed method, by combining FT and PCA, is an effective pattern recognition approach for decomposing the mixed geochemical populations, and for identifying the deep geochemical anomalies. The results obtained from the FT-PCA approach demonstrated that the very

low frequency bands are generally related to the favorable rock types and background values. MPC in this FB represents a very low frequency anomaly, which can be related to the deep geochemical anomaly. The FD analysis of the surface geochemical data for the mineral deposits can provide important insights of the mineral systems and significant implications for mineral exploration.

Table 2. Rotated component matrix in PCA method for frequency bands 1 and 2.

	PCs inFB1							PCs inFB2				
	1	2	3	**4**	5	6		1	2	3	**4**	5
Au	.027	-.135	-.009	.817	-.024	.132	**Au**	.192	.041	.137	.860	.176
Al	.852	.096	-.274	.129	.190	-.093	Al	.872	.344	.218	.208	.037
As	.199	.508	.318	.244	.346	.094	As	.648	.611	.250	.285	-.032
B	.091	.627	.105	.412	.274	.375	B	.640	.618	.297	.306	.027
Ba	-.027	.270	-.414	.538	-.114	-.402	Ba	.145	-.019	-.193	.244	.799
Ca	-.048	-.296	-.030	-.067	.796	.187	Ca	.248	-.041	.758	.169	-.152
Ce	-.149	.912	.082	-.057	-.244	-.005	Ce	.408	.875	-.047	.085	.130
Co	.895	-.078	.024	-.133	.151	-.174	Co	.905	.172	.070	.132	-.201
Cr	.170	.438	.136	.620	.229	-.164	Cr	.635	.555	.228	.362	.086
Cu	-.029	-.089	.257	.870	.005	.230	**Cu**	.406	.382	.243	.758	.036
Fe	-.198	.294	.232	.035	.297	.681	Fe	.574	.633	.365	.292	-.010
Ga	.870	-.074	-.351	.058	-.058	-.092	Ga	.933	.226	.114	.159	.042
K	.170	.008	-.870	.030	.055	.136	K	.698	.127	.333	-.009	.460
La	-.155	.929	.062	-.057	-.142	.038	La	.467	.846	.051	.099	.130
Li	.582	.536	-.063	.402	.285	.065	Li	.745	.543	.243	.271	.054
Mg	.709	.020	-.570	-.021	.296	.003	Mg	.864	.337	.295	.146	.121
Mn	.815	.289	-.021	.325	.116	.054	Mn	.785	.495	.217	.275	-.001
Mo	.148	-.127	-.116	.255	.146	.689	Mo	.649	.488	.388	.280	-.004
Na	-.332	.610	.232	-.294	-.223	.320	Na	.049	.887	.005	-.073	-.044
Ni	.359	.620	.061	.505	.279	.255	Ni	.689	.591	.278	.299	.030
P	-.055	-.224	-.123	.122	.396	.373	P	.195	.079	.774	.093	.034
Pb	.729	-.160	.429	-.107	-.211	-.133	Pb	.566	-.064	-.428	.155	-.578
S	.578	-.092	.018	.017	-.155	.381	S	.757	.459	.259	.245	-.056
Sc	-.067	.171	.803	.176	-.076	.301	Sc	.241	.684	.077	.458	-.403
Sr	.061	-.014	.043	.066	.885	.142	Sr	.618	.399	.536	.280	-.031
Ti	-.124	.323	.761	.172	.233	.074	Ti	.282	.664	.205	.405	-.349
V	-.096	.503	.265	-.054	.176	.760	V	.596	.678	.324	.239	-.035
Y	.256	.785	-.097	-.099	-.225	-.247	Y	.594	.681	-.184	.010	.126
Zn	.828	.080	-.064	.027	-.200	.104	Zn	.842	.434	.113	.206	-.038
Zr	.401	.589	.193	.367	-.241	.058	Zr	.660	.643	.113	.287	.005

Table 3. Rotated component matrix in PCA method for frequency bands 3, 4, 5, and 6.

	PCs inFB3				PCs inFB4				PCs inFB5				PCs inFB6	
	1	2	**3**		1	2	**3**		1	2	**3**		1	**2**
Au	.106	.210	.970	**Au**	.106	.210	.970	**Au**	.104	.207	.971	**Au**	.458	.834
Al	.901	.151	.220	Al	.902	.149	.218	Al	.901	.147	.218	Al	.943	.332
As	.182	.897	.371	As	.182	.898	.369	As	.180	.897	.372	As	.911	.412
B	.348	.361	.862	**B**	.349	.363	.861	**B**	.345	.358	.864	B	.932	.361
Ba	.084	.215	.966	**Ba**	.085	.216	.966	**Ba**	.082	.213	.967	Ba	.939	.343
Ca	.151	.932	.314	Ca	.150	.933	.312	Ca	.148	.932	.314	Ca	.866	.476
Ce	.286	.431	.847	**Ce**	.286	.433	.846	**Ce**	.282	.428	.850	Ce	.943	.331
Co	.291	.764	.567	**Co**	.290	.766	.565	**Co**	.288	.764	.569	Co	.942	.335
Cr	.720	.179	.653	**Cr**	.723	.178	.650	**Cr**	.719	.176	.655	Cr	.938	.347
Cu	.197	.423	.876	**Cu**	.196	.425	.875	**Cu**	.193	.419	.878	**Cu**	.570	.786
Fe	.649	.685	.312	Fe	.648	.687	.310	Fe	.648	.686	.311	Fe	.943	.333
Ga	.803	.454	.372	Ga	.804	.454	.370	Ga	.804	.453	.372	Ga	.944	.330
K	.400	.013	.900	**K**	.403	.011	.899	**K**	.396	.011	.902	K	.942	.336
La	.425	.682	.586	**La**	.424	.684	.584	**La**	.422	.682	.588	La	.943	.331
Li	.835	.302	.453	Li	.837	.302	.450	Li	.835	.300	.454	Li	.938	.346
Mg	.971	.176	.033	Mg	.971	.175	.033	Mg	.971	.174	.031	Mg	.944	.330
Mn	.849	.112	.509	**Mn**	.851	.110	.505	**Mn**	.848	.109	.510	Mn	.934	.356
Mo	.692	.669	.225	Mo	.692	.669	.223	Mo	.692	.669	.223	**Mo**	.076	.958
Na	.676	.686	.178	Na	.676	.687	.177	Na	.675	.688	.175	Na	.939	.343
Ni	.721	.216	.639	**Ni**	.723	.215	.637	**Ni**	.720	.213	.641	Ni	.920	.392
P	.157	.975	.071	P	.157	.975	.072	P	.155	.975	.069	P	.944	.330
Pb	.629	.713	.268	Pb	.628	.714	.267	Pb	.628	.713	.269	Pb	.939	.343
S	.962	.179	.021	S	.962	.178	.020	S	.962	.178	.019	**S**	.497	.793
Sc	.247	.779	.071	Sc	.241	.782	.071	Sc	.243	.780	.068	Sc	.940	.342
Sr	-.002	.926	.370	Sr	-.004	.926	.368	Sr	-.005	.925	.370	Sr	.924	.381
Ti	.270	.618	.725	**Ti**	.269	.621	.723	**Ti**	.269	.615	.727	Ti	.938	.345
V	.714	.657	.131	V	.713	.657	.129	V	.713	.657	.127	V	.940	.342
Y	.374	.884	.245	Y	.372	.886	.245	Y	.371	.886	.244	Y	.945	.328
Zn	.859	.227	.316	Zn	.861	.226	.313	Zn	.858	.225	.316	Zn	.943	.332
Zr	.859	.196	.165	Zr	.860	.195	.163	Zr	.859	.193	.161	Zr	.933	.360

Table 4. Rotated component matrix in PCA method for frequency bands 7, 8, 9, and 10.

	PCs inFB7			PCs inFB8			PCs inFB9			PCs inFB10	
	1	**2**		1	**2**		1	**2**		1	**2**
Au	.459	.833	**Au**	.468	.823	**Au**	.614	.681	Au	.868	.212
Al	.943	.332	Al	.943	.334	Al	.960	.281	Al	.990	.136
As	.911	.412	As	.911	.412	As	.945	.326	As	.986	.169
B	.932	.361	B	.932	.362	B	.955	.298	B	.990	.141
Ba	.939	.343	Ba	.939	.343	Ba	.960	.279	Ba	.992	.123
Ca	.866	.476	Ca	.870	.467	Ca	.942	.303	Ca	.982	.133
Ce	.943	.331	Ce	.943	.333	Ce	.960	.280	Ce	.990	.137
Co	.942	.336	Co	.941	.337	Co	.959	.285	Co	.990	.138
Cr	.938	.347	Cr	.937	.348	Cr	.956	.293	Cr	.989	.148
Cu	.571	.786	**Cu**	.576	.781	**Cu**	.678	.684	Cu	.863	.359
Fe	.943	.334	Fe	.942	.335	Fe	.960	.281	Fe	.991	.136
Ga	.944	.330	Ga	.943	.332	Ga	.960	.279	Ga	.991	.135
K	.942	.336	K	.942	.337	K	.961	.276	K	.991	.134
La	.943	.331	La	.943	.333	La	.960	.280	La	.990	.136
Li	.938	.346	Li	.938	.348	Li	.957	.289	Li	.990	.137
Mg	.944	.330	Mg	.943	.331	Mg	.961	.277	Mg	.991	.133
Mn	.934	.356	Mn	.934	.357	Mn	.955	.296	Mn	.990	.143
Mo	.076	.958	**Mo**	.073	.957	**Mo**	.056	.952	**Mo**	.113	.990
Na	.939	.343	Na	.939	.343	Na	.960	.279	Na	.991	.129
Ni	.920	.392	Ni	.919	.393	Ni	.944	.330	Ni	.985	.174
P	.944	.330	P	.943	.332	P	.960	.279	P	.990	.136
Pb	.939	.343	Pb	.939	.344	Pb	.960	.281	Pb	.992	.126
S	.499	.791	**S**	.521	.773	S	.810	.447	S	.917	.275
Sc	.939	.342	Sc	.939	.343	Sc	.957	.289	Sc	.989	.149
Sr	.924	.381	Sr	.924	.379	Sr	.959	.282	Sr	.992	.122
Ti	.938	.345	Ti	.938	.345	Ti	.959	.282	Ti	.991	.137
V	.939	.342	V	.939	.343	V	.958	.285	V	.990	.141
Y	.944	.328	Y	.944	.330	Y	.960	.278	Y	.990	.136
Zn	.943	.332	Zn	.943	.333	Zn	.961	.277	Zn	.991	.129
Zr	.933	.360	Zr	.932	.361	Zr	.952	.306	Zr	.986	.164

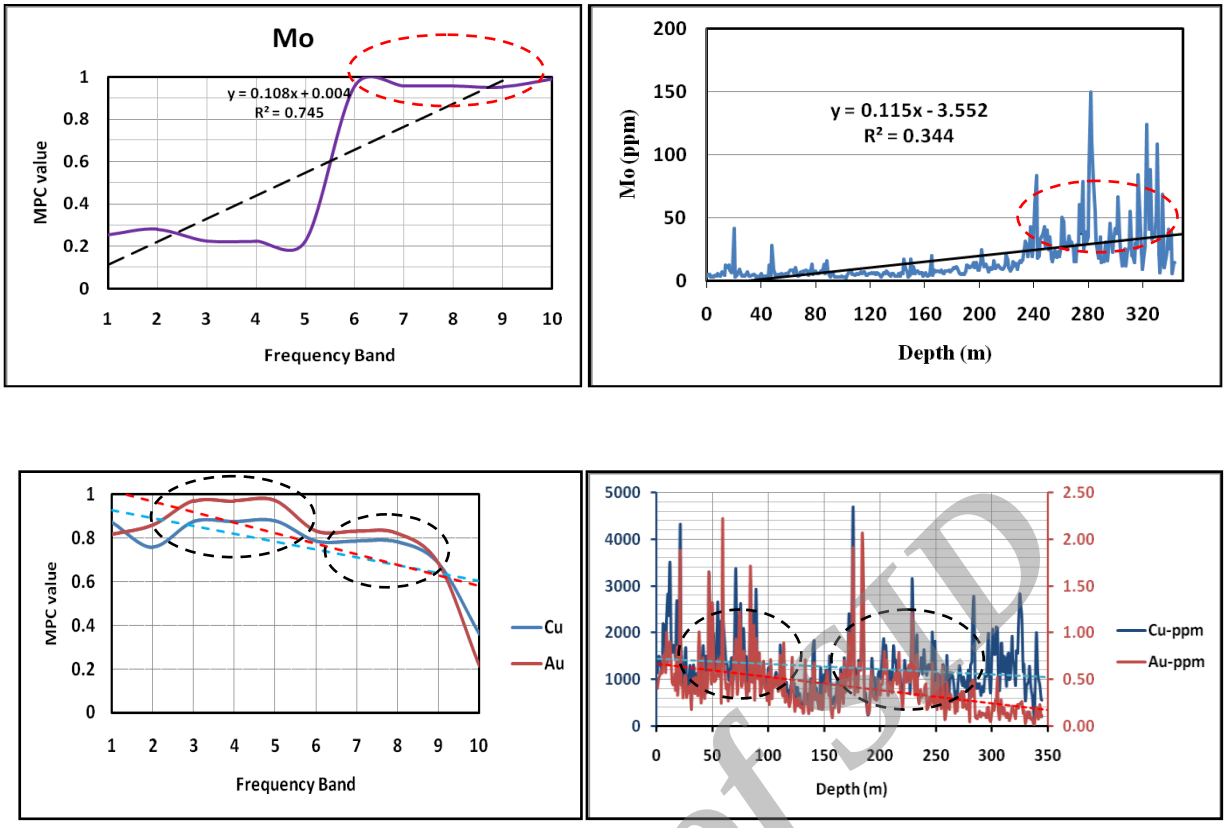

Figure 5. Diagrams of MPC values *vs.*FBs comparing with variations in Mo, Au and Cu values and their trends in borehole DDH03.

The increasing and decreasing trends of MPC values diagram in FD can provide a basis for the development and application of this approach for exploration of the hidden mineral deposits. The introduced technique can identify the blind mineralization, and predict the variation in mineralization in depth without exploration drilling. Finally, this finding shows a possibility for an extensive mineralization in this area. The presented methodology, which is based on 2D-FT, is quite inexpensive compared to the traditional exploration methods.

5. Conclusions

The results obtained from the newly developed approach that is based on coupling 2D-FT and PCA revealed significant and valuable exploratory information that were not achievable in the spatial domain. The introduced technique makes it possible, without exploration drilling, to identify the deep and blind mineralization, and predict the variation in mineralization in the depth. This idea demonstrated that there was a direct relationship between the deposit depth and the frequencies of the surface geochemical distribution maps. The high frequencies in the surface geochemical distribution maps may be related to the surface anomalies and geochemical noises. Very low frequencies can relate to the background values and very deep geochemical anomalies. The MPC coefficients in the rotated component matrix in the PCA method can show the importance and intensity of the elements in a mineral deposit. The diagram of the MPC values *vs.*FBs can show the variability of anomalies in the deferent depth. The mineralization sequence of Au (Cu)→Cu (Au)→Mo from surface to depth, and the mineralization zones to the wall rock in the Dalli area, were properly and clearly predicted in the MPC values diagrams. There was a deep Mo geochemical anomaly from 240m to down in the borehole that was predicted in the MPC values diagram. The MPC values for Cu and Au were shown to correspond to two peaks for the high and intermediate FBs related to the surface and deep anomalies. The high correlation between Cu and Au in the MPC diagram is related to their correlation in the hypogene and supergene zones. The proposed valuable method was an effective pattern recognition approach for decomposing mixed geochemical populations, and for identifying deep geochemical anomalies.

References

[1]. Afzal, P., Fadakar Alghalandis, Y., Moarefvand, P., Rashidnejad Omran, N. and Asadi Haroni, H. (2012). Application of power-spectrum–volume fractal method for detecting hypogene, supergene enrichment, leached and barren zones in Kahang Cu porphyry deposit,Central Iran, Journal of Geochemical Exploration. 112: 131-138.

[2]. Cao, L. and Cheng, Q. (2012). Quantification of anisotropic scale invariance of geochemical anomalies associated with Sn-Cu mineralization in Gejiu, Yunan Province, China, Geochemical Exploration. 122: 47-54.

[3]. Cheng, Q. and Zhao, P. (2011). Singularity theories and methods for characterizing mineralization processes and mapping geo-anomalies for mineral deposit prediction. Geoscience Frontiers. 2 (1): 67-79.

[4]. Zuo, R. (2011). Identifying geochemical anomalies associated with Cu and Pb–Zn skarn mineralization using principal component analysis and spectrum–area fractal the Gangdese Belt, Tibet (China). J. Geochemical Exploration. 111: 13-22.

[5]. Zuo, R. (2011). Decomposing of mixed pattern of arsenic using fractal model in Gangdese belt, Tibet, China. Applied Geochemistry. 26: S271-S273.

[6]. Hassani, H., Daya, A. and Alinia, F. (2009). Application of a fractal method relating power spectrum and area for separation of geochemical anomalies from background. Aust J Basic Appl Sci. 3 (4): 3307-3320.

[7]. Cheng, Q., Xu, Y. and Grunsky, E. (2000). Integrated Spatial and Spectrum Method for Geochemical Anomaly Separation, Natural Resources Research. 9 (1).

[8]. Cheng, Q. (1999). Spatial and scaling modelling for geochemical anomaly separation. Journal of Geochemical Exploration. 65: 175-194.

[9]. Zuo, R., Carranza, E.J.M. and Cheng, Q. (2012). Fractal/multifractal modelling of geochemical exploration data. Journal of Geochemical Exploration. 122: 1-3.

[10]. Zuo, R., Xia, Q. and Zhang, D. (2013). A comparison study of the C-A and S-A models with singularity analysis to identify geochemical anomalies in covered areas. Applied Geochemistry. 33: 165-172.

[11]. Grigorian, S.V. (1985). Secondary Lithochemical Halos in Prospecting for Hidden Mineralization.Nedra Publishing House, Moscow.

[12]. Grigorian, S.V. (1992). Mining Geochemistry.Nedra Publishing House, Moscow.

[13]. Levinson, A.A. (1980). Introduction to Exploration Geochemistry.Applied Publishing Ltd., Wilmette, USA.

[14]. Ziaii, M., Abedi, A. and Ziaii, M. (2007). Prediction of hidden ore bodies by new integrated computational model in marginal Lut region in east of Iran. In: Milkereit, B. (Ed.), Proc. Exploration 07: Fifth Decennial Internat. Conf. Mineral Exploration, Toronto, Canada, pp. 957-961.

[15]. Ziaii, M., Pouyan, A.A. and Ziaei, M. (2009). Neuro-fuzzy modelling in mining geochemistry: Identifications of geochemical anomalies, Journal of Geochemical Exploration, 100: 25-26.

[16]. Ziaii, M., Carranza, E.J.M. and Ziaei, M. (2011). Application of geochemical zonality coefficients in mineral prospectivity mapping.Comput.Geosci. 37: 1935-1945.

[17]. Ziaii, M., Doulati, F., Ziaei, M. and Soleymani, A. (2012). Neuro-fuzzy modeling based genetic algorithms for identification of geochemical anomalies in mining geochemistry. J. Applied Geochemistry. 27: 663-676

[18]. Cheng, Q., Jing, L. and Panahi, A. (2006). Principal component analysis with optimum order sample correlation coefficient for image enhancement. International Journal of Remote Sensing. 27 (16): 3387–3401.

[19]. Davis, J.C. (2002). Statistics and Data Analysis in Geology, 3rd ed., John Wiley & Sons Inc., NewYork, 550 p.

[20]. Garrett, R.G. and Grunsky, E.C. (2001). Weighted sums—knowledge based empirical indices for use in exploration geochemistry. Geochemistry: Exploration Environment Analysis1. 135–141.

[21]. Chandrajith, R., Dissanayake, C.B. and Tobschall, H.J. (2001). Application of multi-element relationships in stream sediments to mineral exploration: a case study of Walawe Ganga Basin, Sri Lanka. Applied Geochemistry 16 (3): 339-350.

[22]. Cheng, Q., Bonham-Carter, G., Wang, W., Zhang, S., Li, W. and Xia, Q. (2011). A spatially weighted principal component analysis for multi-element geochemical data for mapping locations of felsic intrusions in the Gejiu mineral district of Yunnan, China. Computer & Geosciences. 37: 662-669.

[23]. Loughlin, W. P. (1991). Principal component analysis for alteration mapping. Photogrammetric Engineering and Remote Sensing. 57 (9): 1163-1169.

[24]. Zhao, J., Wang, W., Dong, L., Yang, W., and Cheng, Q. (2012). Application of geochemical anomaly identification methods in mapping of intermediate and felsic igneous rocks in eastern Tianshan, China. Journal of Geochemical Exploration. 122: 81-89.

[25]. Darabi-Golestan, F., Ghavami-Riabi, R. and Asadi-Harooni, H. (2013). Alteration, zoning model, and mineralogical structure considering lithogeochemical investigation in Northern Dalli Cu–Au porphyry. Arabian Journal of Geosciences. 6(12): 4821-4831.

[26]. Yousefifar, S., Khakzad, A., Asadi Harooni, H., Karami, J., Jafari, M.R. and Vosoughi Abedin, M. (2011). Prospecting of Au and Cu bearing targets by exploration data combination in southern part of Dalli Cu-Au porphyry deposit, central Iran. Archives of Mining Sciences. 56: 21-34.

[27]. Asadi Haroni, H. (2008). First stage drilling report on Dalli porphyry Cu– Au prospect, Central Province of Iran, Technical Report.

[28]. Cios, K.J., Swiniarski, R.W., Pedrycz, W. and Kurgan, L.A. (2007). The knowledge discovery process.In Data Mining (pp. 9-24). Springer US.

[29]. Cheng, Q. (2006). Multifractal modelling and spectrum analysis of gamma ray spectrometer data from southwestern Nova Scotia, Canada, Science in China. 49 (3): 283-294.

[30]. Cheng, Q., Xu, Y. and Grunsky, E. (1999). Integrated spatial and spectral analysis for geochemical anomaly separation. In: Lippard, S.J., Naess, A., Sinding-Larsen, R. (Eds.),Proceedings of the Fifth Annual Conference of the International Association for Mathematical Geology, Trondheim, Norway 6-11th August, Vol. 1, pp. 87–92.

[31]. Dobrin, M.B. and Savit, C.H. (1988). Geophysical propecting: McGraw-Hill Book Co., New York, 867 P.

[32]. Bhattacharyya, B.K. (1966). Continuous spectrum of the total-magnetic-field anomaly due to a rectangular prismatic body. Geophysics. 31(1): 97-121.

[33]. Gonzalez, R.C. and Woods, R.E. (2002). Digital image processing.Prentice-Hall, Upper Saddle River, NJ, 793 pp.

[34]. Ge, Y., Cheng, Q. and Zhang, S. (2005). Reduction of edge effects in spatial information extraction from regional geochemical data: a case study based on multifractal filtering technique, Computers & Geosciences. 31: 545-554.

[35]. Cheng, Q. and Xu, Y. (1998). Geophysical data processing and interpreting and for mineral potential mapping in GIS environment.In Proceedings of the Fourth Annual Conference of the International Association for Mathematical Geology. 2: 394-399.

پیش‌بینی مدل ذخیره معدنی و شناسایی روند کانی‌سازی در عمق با استفاده از حوزه فرکانس داده‌های ژئوشیمیایی سطحی در ذخیره مس- طلای پورفیری دالی

حسین شاهی[1*]، رضا قوامی ریابی[1]، ابوالقاسم کامکار روحانی[1] و هوشنگ اسدی هارونی[2]

۱- دانشکده مهندسی معدن، نفت و ژئوفیزیک، دانشگاه صنعتی شاهرود، ایران

۲- دانشکده مهندسی معدن، دانشگاه صنعتی اصفهان، ایران

ارسال ۲۰۱۴/۱۱/۱۲، پذیرش ۲۰۱۵/۴/۶

* نویسنده مسئول مکاتبات: hssn.shahi@gmail.com

چکیده:

در این تحقیق به‌منظور تجزیه الگوهای پیچیده ژئوشیمیایی مربوط به اعماق مختلف ذخیره معدنی، حوزه فرکانس داده‌های ژئوشیمیایی سطحی مورد تحلیل قرار گرفت. به‌منظور پیش‌بینی تغییرات کانی‌سازی در عمق و شناسایی آنومالی‌های ژئوشیمیایی عمیق و کانی‌سازی پنهان با استفاده از داده‌های ژئوشیمیایی سطحی در کانسار مس- طلای پورفیری دالی، یک روش پیشرفته بر اساس ترکیب روش‌های تبدیل فوریه و تحلیل مؤلفه‌های اصلی پیشنهاد شد. داده‌های ژئوشیمیایی سطحی با استفاده از تبدیل فوریه به حوزه فرکانس انتقال داده شد و فیلترهای بالا گذر و پایین گذر بر روی داده‌های حوزه فرکانس انجام شد سپس روش تحلیل مؤلفه‌های اصلی به‌صورت جداگانه بر روی این باندهای فرکانسی اعمال گردید. این روش جدید ترکیبی، ارتباط بین فرکانس‌های بالا و پایین در نقشه توزیع ژئوشیمیایی سطحی را با عمق کانسار به خوبی نشان داد. این روش ترکیبی یک ابزار ارزشمند برای پردازش داده و تشخیص الگو جهت شناسایی آنومالی‌های پنهان و تعیین روندهای کانی‌سازی در عمق بدون استفاده از حفاری است. اطلاعات به‌دست‌آمده از حفاری‌های اکتشافی مانند گمانه‌ها، نتایج حاصل از این روش را تأیید می‌کند. اطلاعات اکتشافی به‌دست‌آمده از حوزه فرکانس نقشه توزیع ژئوشیمیایی سطحی، در حوزه مکان قابل دست‌یابی نیست. این روش در مقایسه با روش‌های اکتشافی سنتی کاملاً ارزان‌تر است.

کلمات کلیدی: تحلیل مؤلفه‌های اصلی، حوزه فرکانس، تبدیل فوریه دوبعدی، کانی‌سازی پنهان، تشخیص الگو.